Antiferromagnetic classical XY model: A mean-field analysis

D. H. Lee, R. G. Caflisch, and J. D. Joannopoulos
Department of Physics, Massachusetts Institute of Technology, Cambridge, Massachusetts 02139

F. Y. Wu*
Division of Materials Research, National Science Foundation, Washington, D. C. 20550
(Received 1 September 1983)

The antiferromagnetic classical XY (planar-rotator) model is analyzed under the mean-field approximation. Phase diagrams are obtained and found to be strongly dependent on the underlying lattice geometry. For bipartite lattices, there exists a second-order transition across a unique phase boundary. For tripartite lattices, there exist two phase boundaries, separating an intermediate "nonhelical" phase from a low-temperature "helical" phase and the high-temperature paramagnetic phase. The two phase boundaries merge into a single critical point at finite temperature and zero magnetic field.

I. INTRODUCTION

Critical properties of the two-dimensional ferromagnetic classical XY model, also known as the planar-rotator model, are now well understood as a result of the seminal studies carried out by Kosterlitz and Thouless.[1-3] In contrast, however, there have been few studies done on the planar-rotator model with antiferromagnetic interactions. Recent Monte Carlo simulations[4] suggest that the nature of phase transitions in such systems is affected by the introduction of frustration. This implies that for an antiferromagnetic Hamiltonian, the underlying lattice structure is important. Further studies are very much needed to clarify the situation. Here we take the underlying lattice geometry explicitly into account and report the results of a mean-field analysis of the antiferromagnetic planar-rotator model for bipartite (e.g., square) and tripartite (e.g., triangular) lattices.[5] This provides a set of exactly solvable equations determining the free energy and hence all the thermodynamic properties of the system.

We find that there indeed exist profound differences in the critical properties of the bipartite and tripartite lattices, even under the mean-field approximation. Briefly, the H-T phase diagram for bipartite lattices, where T is the temperature and H is a uniform magnetic field, is found to consist of a single phase boundary separating an ordered phase from the paramagnetic phase. The transition across this phase boundary is second order. For tripartite lattices, however, the phase diagram has a different structure. For temperature T below a critical value, the system undergoes a sequence of two transitions as the magnetic field is increased, from a "helical" phase to a "nonhelical" phase, and finally to the paramagnetic phase. The transition is second order across the paramagnetic boundary, but the nature of the helical-to-nonhelical transition is more subtle and will be discussed in detail in Sec. III. Above the critical temperature the system remains paramagnetic regardless of the lattice geometry.

The format of this paper is as follows. In Sec. II we describe the mean-field-theory formalism and obtain its solution. In Sec. III we present an analysis of the results and in Sec. IV we make some concluding remarks.

II. FORMALISM

Consider an antiferromagnetic classical XY model defined by the reduced Hamiltonian

$$\mathscr{H}=K\sum_{\langle i,j\rangle}\vec{s}_i\cdot\vec{s}_j-\vec{h}\cdot\sum_i\vec{s}_i\ , \tag{1}$$

where $K\equiv J/(k_BT)>0$, $\vec{h}\equiv\vec{H}/(k_BT)$, and the summations are extended over the sites of a lattice whose coordination number is z. Here $\langle i,j\rangle$ denotes nearest neighbors, and the spins are unit vectors confined in a plane (planar rotator). Writing $\vec{h}\cdot\vec{s}_i=h\cos\theta_i$ where θ_i is the angle between the spin $\vec{s}_i$ and the applied field $\vec{H}$, the Hamiltonian (1) can also be written as

$$\mathscr{H}=K\sum_{\langle i,j\rangle}\cos(\theta_i-\theta_j)-h\sum_i\cos\theta_i\ . \tag{2}$$

Consider first the ground state of the Hamiltonian for $h=0$. For bipartite lattices the spins on the two sublattices are aligned in opposite directions. For tripartite lattices, the ground state consists of configurations in which spins on different sublattices form $\pm120°$ angles with each other. In particular, for the triangular lattice this leads (up to a global-spin-rotational degeneracy) to a $\sqrt{3}\times\sqrt{3}$ periodic pattern shown in Fig. 1. We note that there exists two topologically distinct[6] ground-state patterns described by different "helicity." To each elementary triangle in Fig. 1 we assign a helicity, + or −, according to the way that the three spins at the vertices of the triangle are aligned. A + (−) helicity describes an arrangement in which the spins are rotated sequentially 120° clockwise (counterclockwise) when the triangle is traversed in a clockwise direction.[7] This discrete degeneracy in helicity is one of the most interesting and profound differences between bipartite and tripartite systems.

The mean-field calculation is performed by minimizing the following free-energy functional:[8]

 ©1984 The American Physical Society

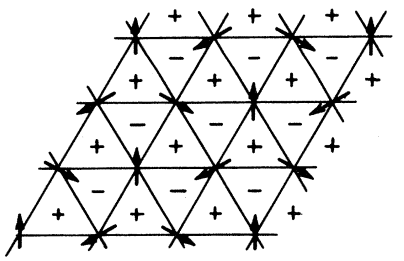

(a)

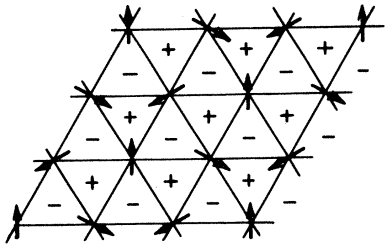

(b)

FIG. 1. Typical ground-state patterns for the triangular lattice at $H=0$. The plus or minus signs indicate the helicity of each triangle. The pattern shown in (b) can be obtained from the pattern shown in (a) by a reflection.

$$\Psi[\rho]=\mathrm{Tr}(\rho\mathscr{H}+\rho\ln\rho) \tag{3}$$

under the constraint

$$\rho=\prod_i \rho_i \ , \tag{4}$$

where Tr designates the trace over all states of the system, and ρ_i is the density matrix of site i. Substitution of (2) and (4) into (3) gives, with $\mathrm{Tr}\rho_i=1$,

$$\Psi[\rho_i]=K\sum_{\langle i,j\rangle}(C_iC_j+S_iS_j)-h\sum_i C_i+\sum_i \mathrm{Tr}(\rho_i\ln\rho_i) \ , \tag{5}$$

where

$$C_i\equiv\mathrm{Tr}(\rho_i\cos\theta_i), \quad S_i\equiv\mathrm{Tr}(\rho_i\sin\theta_i) \ . \tag{6}$$

Clearly C_i and S_i are the respective mean values of the spin components in directions parallel and perpendicular to the applied field. The variational equations are given by

$$-K\sum_j{}'(C_j\cos\theta_i+S_j\sin\theta_i)+h\cos\theta_i+\lambda_i-1=\ln\rho_i(\theta_i) \tag{7}$$

for all i, where λ_i is the Lagrange multiplier introduced to ensure the normalization of ρ_i. The prime in (7) designates that j is the nearest neighbor of i. If one exponentiates (7), collects the coefficients of the $\cos\theta_i$ and $\sin\theta_i$ terms, and removes λ_i through the normalization condition, one can show that

$$\rho_i(\theta_i)=\frac{1}{2\pi I_0(a_i)}e^{a_i\cos(\theta_i-\phi_i)} \ , \tag{8}$$

where

$$a_i\cos\phi_i\equiv h-K\sum_j{}'C_j, \quad a_i\sin\phi_i\equiv -K\sum_j{}'S_j \ , \tag{9}$$

and

$$I_\nu(a)\equiv(2\pi)^{-1}\int_0^{2\pi}\cos(\nu\theta)e^{a\cos\theta}d\theta$$

is the modified Bessel function of the first kind of integer order ν. In (8), a_i and ϕ_i can be interpreted as the magnitude and the angle of the local mean field on site i. Substituting (8) into (6) one obtains

$$C_i=R(a_i)\cos\phi_i, \quad S_i=R(a_i)\sin\phi_i \tag{10}$$

both for all i, where $R(a)\equiv I_1(a)/I_0(a)$. Substituting (10) into (9) yields the following self-consistent equations for determining a_i and ϕ_i:

$$\begin{aligned} &K\sum_j{}'R(a_j)\cos\phi_j+a_i\cos\phi_i=h \ , \\ &K\sum_j{}'R(a_j)\sin\phi_j+a_i\sin\phi_i=0 \ , \end{aligned} \tag{11}$$

both for all i. The extremum free energy is given by

$$\begin{aligned} \Psi(a_i,\phi_i)=&K\sum_{\langle i,j\rangle}R(a_i)R(a_j)\cos(\phi_i-\phi_j) \\ &-h\sum_i R(a_i)\cos\phi_i \\ &+\sum_i\{a_iR(a_i)-\ln[2\pi I_0(a_i)]\} \ , \end{aligned} \tag{12}$$

where the a_i's and ϕ_i's are the solutions of (11). Equation (11) is most general, and for a system of N sites, it represents a set of $2N$ equations. The number of independent equations is reduced drastically if one takes into account the fact that both the ground state and the disordered state have the sublattice periodicity. Thus, for an n-partite lattice of coordination number z, (11) reduces to $2n$ equations,

$$\begin{aligned} &Kq\sum_{\substack{\beta=1\\ \beta\neq\alpha}}^{n}R(a_\beta)\cos\phi_\beta=h-a_\alpha\cos\phi_\alpha \ , \\ &Kq\sum_{\substack{\beta=1\\ \beta\neq\alpha}}^{n}R(a_\beta)\sin\phi_\beta=-a_\alpha\sin\phi_\alpha \ , \end{aligned} \tag{13}$$

for $\alpha=1,\ldots,n$, where $q\equiv z/(n-1)$ is the number of nearest neighbors (of any given site) belonging to the same sublattice. The extremum free energy per spin is now given by

$$\begin{aligned} \psi(a_\alpha,\phi_\alpha)=&\frac{q}{2n}K\sum_{\alpha=1}^{n}\sum_{\substack{\beta=1\\ \beta\neq\alpha}}^{n}R(a_\alpha)R(a_\beta)\cos(\phi_\alpha-\phi_\beta) \\ &-\frac{h}{n}\sum_{\alpha=1}^{n}R(a_\alpha)\cos\phi_\alpha \\ &+\frac{1}{n}\sum_{\alpha=1}^{n}\{a_\alpha R(a_\alpha)-\ln[2\pi I_0(a_\alpha)]\} \ . \end{aligned} \tag{14}$$

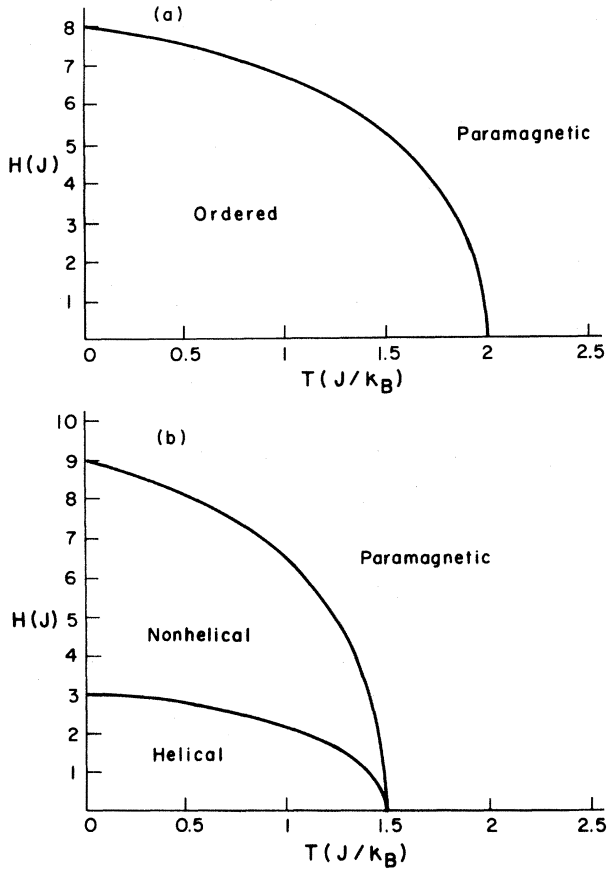

FIG. 2. Phase diagrams of (a) the square and (b) the triangular antiferromagnetic XY model. In (b) there are two ordered phases (helical and nonhelical) and a paramagnetic phase. At zero field the phase boundaries merge into a single critical point.

Our task is to find all possible solutions of (13) and determine which solution corresponds to the lowest free energy through (14). In this way we can determine the stable phase of the system for different $T\ [=J/(k_BK)]$ and H (equal to h/K) and therefore construct the entire phase diagram.

III. RESULTS

Let us now be specific to the square ($n=2$, $z=4$, $q=4$) and triangular ($n=3$, $z=6$, $q=3$) lattices. The phase diagrams are shown in Fig. 2. The paramagnetic phase for both lattices corresponds to a solution of (13) of the form

$$\phi_\alpha=0,\quad a_\alpha=a_0(K,h)\quad \text{for } \alpha=1,\ldots,n\ , \tag{15}$$

where

$$a_0+KzR(a_0)=h\ . \tag{16}$$

For the ordered phases one obtains

$$\phi_\alpha=\omega_\alpha,\quad a_\alpha=a_0'(K)\neq 0\quad \text{for } \alpha=1,\ldots,n\ , \tag{17}$$

where

$$a_0'-KqR(a_0')=0\ , \tag{18}$$

and

$$\sum_{\alpha=1}^{n}\cos\omega_\alpha=\frac{1}{qR(a_0')}\frac{h}{K},\quad \sum_{\alpha=1}^{n}\sin\omega_\alpha=0\ . \tag{19}$$

Whereas (16) has a unique solution for any K and h, (18) can have *two* solutions ($a_0'=0$ and $a_0'\neq 0$) in a specific range of K. This is illustrated in Fig. 3. Since the slope of $R(a)$ is $\frac{1}{2}$ at $a=0$, the specific temperature range is given by $0<1/K<q/2$. Therefore, the ordered phases only exist for $0<1/K<q/2$. Moreover, from (19) we note that the ordered phases can only exist for $h\leq nqKR(a_0'(K))$. The graphical solution of (19) for various values of $h/[qR(a_0')K]$ is shown in Fig. 4 for the square and the triangular lattice. In this figure each vector represents $\vec{u}_\alpha\equiv(\cos\omega_\alpha,\sin\omega_\alpha)$ and (19) requires

$$\sum_{\alpha=1}^{n}\vec{u}_\alpha=(h/[qR(a_0')K],\,0)\ .$$

With this picture in mind, we draw two unit circles whose centers are at a distance h/qKR apart and whose radii are $\vec{u}_1$ and $\vec{u}_n$, respectively. Then, as shown in Fig. 4(a), this procedure uniquely determines the vectors $\vec{u}_1$ and $\vec{u}_2$ for $n=2$, but leads to an infinite set of solutions for $n=3$. The paramagnetic phase boundaries correspond to the loci of T and H satisfying

$$h=KnqR(a_0'(K))\ . \tag{20}$$

Substituting (20) into (16) yields

$$a_0+KzR(a_0)=a_0'+KzR(a_0') \tag{21}$$

or

$$a_0(K,h)=a_0'(K)\ . \tag{22}$$

Substituting (20) into (19) yields

$$\sum_{\alpha=1}^{n}\cos\omega_\alpha=n,\quad \sum_{\alpha=1}^{n}\sin\omega_\alpha=0\ , \tag{23}$$

or

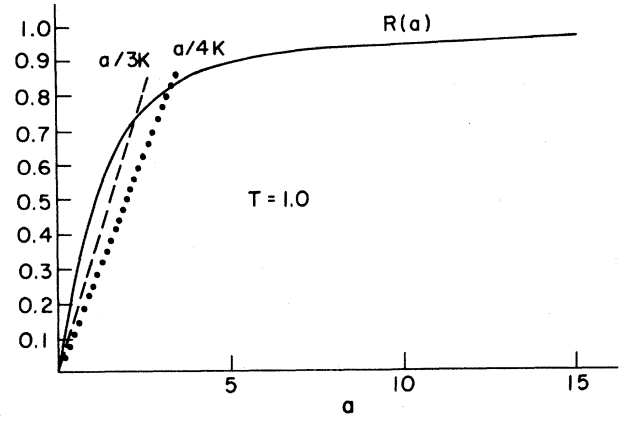

FIG. 3. Graphical solution of (18) at $T=J/k_B<T_c$. The solid curve represents $R(a)$ and the dashed and dotted lines represent $a/(3K)$ and $a/(4K)$, respectively.

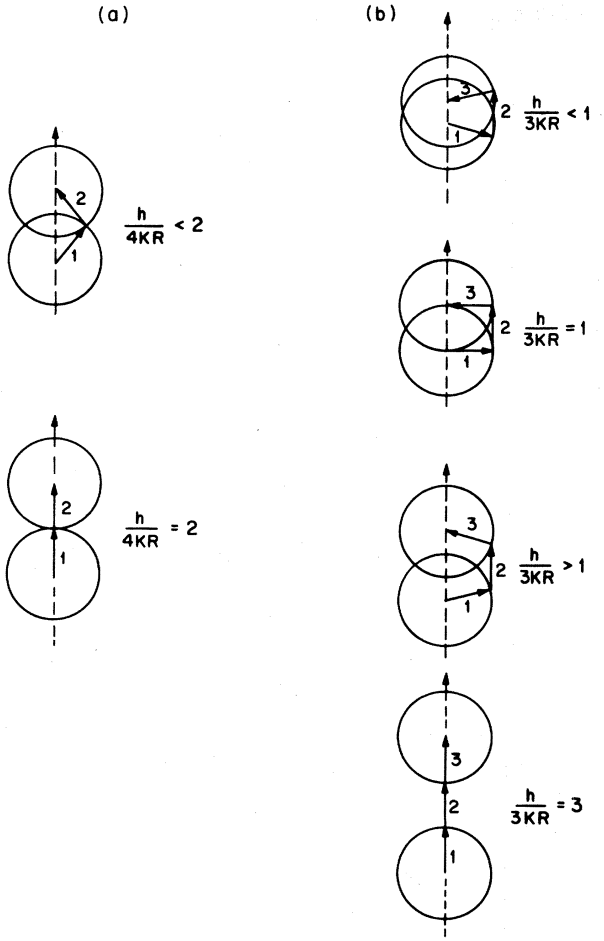

FIG. 4. Graphical solution of (19). (a) Square lattice. (b) Triangular lattice. The vector $\vec{u}_\alpha$ is denoted by α. The solution in (a) is twofold degenerate, and an infinite set of solutions to (b) is generated by sliding the vector labeled 2 along the tracks defined by the two circles. The helicity of the solution in (b) changes at $h/(3KR)=1$.

$$\omega_\alpha=0, \quad \alpha=1,\ldots,n \ . \tag{24}$$

Equations (22) and (24) together imply that both the magnitude (a_α) and the angle (ω_α) of the mean sublattice magnetization change continuously across the outer phase boundary, thereby indicating a continuous transition. Moreover, we have calculated the specific heat and found a discontinuity across the paramagnetic phase boundary suggesting that the transition is second order.

The additional (inner) phase boundary of the triangular lattice phase diagram satisfies

$$h=3KR(a_0'(K)) \ . \tag{25}$$

To understand the nature of the inner boundary consider the following. In the first panel of Fig. 4(b), $h/[3KR(a_0')]$ is less than unity. We note that the three vectors shown in this panel correspond to a spin configuration of the system exhibiting a pattern of alternating helicity similar to those shown in Fig. 1. In addition, one can generate an opposite-helicity spin pattern simply by reflecting the three vectors across the dashed line. A continuous manifold of solutions can be generated if one "slides" the two ends of the second vector on the "tracks" defined by the two circles. Moreover, one can prove that this operation can never change the helicity of any triad. In the third panel of Fig. 4(b), $h/[3KR(a_0')]$ is greater than unity. In this case all solutions correspond to zero-helicity spin patterns and one can always reach the mirror reflected solution through "sliding." The inner phase boundary shown in Fig. 2(b) corresponds to the second panel shown in Fig. 4(b) where $h/[3KR(a_0')]=1$. Since in mean-field theory any two solutions related by sliding have the same free energy, one would expect that in the real system there exists arbitrarily low energy excitations constructed by long-wavelength spatial distortions of the spins so that locally

$$\cos\omega_1+\cos\omega_2+\cos\omega_3=h/[3KR(a_0')] \tag{26}$$

and

$$\sin\omega_1+\sin\omega_2+\sin\omega_3=0 \ . \tag{27}$$

At finite temperature these excitations can sufficiently mix mean-field solutions in the same continuum, so that within the inner phase boundary there will be two coexisting phases of opposite helicity, but outside of the inner phase boundary there will be only one phase of zero helicity. Furthermore, one would expect the inner phase transition to be associated with the vanishing of the interface tension. Under such conditions, the wall formed at the interface of two semi-infinite domains, which have opposite helicity, becomes thermodynamically favorable. As usual, the real transition temperature should be lower than the value predicted by the mean-field theory. As shown in Fig. 2(b), when the magnetic field vanishes, the two phase boundaries *merge* and coalesce to a single critical point on the temperature axis. It is conceivable that this may give rise to a new type of critical point. Finally, we emphasize that an interesting feature of the triangular lattice is the presence of a continuous ground-state degeneracy even for a nonzero magnetic field (which removes the global-spin-rotational symmetry). This "accidental degeneracy" is absent in the square lattice.

IV. CONCLUDING REMARKS

We have described the mean-field phase diagram of bipartite and tripartite antiferromagnetic *XY* models using the square and triangular lattices as specific examples. The results exhibit intriguing differences between these two types of systems. For the square lattice the phase diagram consists of an ordered phase and a paramagnetic phase. For the triangular lattice, there are three different phases: the helical phase, the nonhelical phase, and the paramagnetic phase. Since our mean-field theory is exact at $T=0$, the existence of three different phases is rigorously proved. The phase boundaries separating the helical and nonhelical phases and the nonhelical and paramagnetic phases merge at $H=0$. A plausible conjecture is that there may be a new universality class associated with this critical point. The ground states for the square and the triangular lattices also show very interesting differences. At $H=0$ the ground state of the square lattice breaks global-spin-rotational symmetry, whereas the ground state

of the triangular lattice breaks an additional reflection symmetry. At finite H the continuous symmetry of the Hamiltonian is removed for both systems. The ground state for the square lattice is therefore only twofold degenerate (the remaining degeneracy is due to the symmetry involving a global spin reflection about the axis defined by the external field); however, the ground state of the triangular lattice remains *continuously* degenerate.

In order to determine the nature of the phase diagram more quantitatively, one needs to include the effects of fluctuations. This can be done by performing Monte Carlo calculations throughout the entire H-T plane. Such calculations are currently in progress and will be reported elsewhere.[9]

ACKNOWLEDGMENTS

We would like to thank A. N. Berker, D. Landau, J. Negele, and M. Kardar for helpful discussions. This work was supported in part by the U.S. Office of Naval Research under Grant No. N00014-77-C-0132. One of us (R.G.C.) would like to thank the Fannie and John Hertz Foundation for a fellowship. The research of another of us (F.Y.W.) was performed as part of the National Science Foundation (NSF) Independent Research Program. However, any of the opinions expressed herein are those of the author and do not necessarily reflect the views of the NSF.

---

*Permanent address: Department of Physics, Northeastern University, Boston, MA 02115.

[1]J. M. Kosterlitz and D. J. Thouless, J. Phys. C 5, 124 (1972).

[2]J. M. Kosterlitz and D. J. Thouless, J. Phys. C 6, 1181 (1973).

[3]J. M. Kosterlitz, J. Phys. C 7, 1046 (1974).

[4]S. Teitel and C. Jayapraskash, Phys. Rev. B 27, 598 (1983).

[5]A lattice is n-partite if there are n *equivalent* sublattices for which spins on the same sublattice do not interact.

[6]This means that no continuous transformation of the spins can both keep the configuration a ground state and connect these two states.

[7]The helicity can be defined more generally as $\Delta\theta/2\pi$, where $\Delta\theta$ is the total clockwise change in angle when each triangle is traversed in a clockwise fashion. At each individual step the smallest possible change in angle is chosen.

[8]H. Falk, Am. J. Phys. 38, 858 (1970).

[9]D. H. Lee, J. D. Joannopoulos, J. Negele and D. Landau (unpublished).